V. Motta, L. Malzacher, V. Bicalho Civinelli de Almeida, T.D. Phan, R. Liebich, D. Peitsch, G. Quaranta
A Physically Consistent Reduced Order Model for Plasma Aeroelastic Control on Compressor Blades
Journal of Engineering for Gas Turbines and Power, Vol. 141, N. 9, 2019, 091001
(13 pages)
doi:10.1115/1.4043545

A PHYSICALLY CONSISTENT REDUCED ORDER MODEL FOR PLASMA AEROELASTIC CONTROL ON COMPRESSOR BLADES

Valentina Motta
valentina.motta@tu-berlin.de*
Dept. of Aeronautics and Astronautics
Technische Universität Berlin
Berlin, Germany

Leonie Malzacher
leonie.malzacher@tu-berlin.de
Dept. of Aeronautics and Astronautics
Technische Universität Berlin
Berlin, Germany

Victor Bicalho Civinelli de Almeida
Victor.Bicalho@ilr.tu-berlin.de
Dept. of Aeronautics and Astronautics
Technische Universität Berlin
Berlin, Germany

Tien Dat Phan
t.phan@tu-berlin.de
Dept. of Machine Design
Technische Universität Berlin
Berlin, Germany

Robert Liebich
Robert.Liebich@tu-berlin.de
Dept. of Machine Design
Technische Universität Berlin
Berlin, Germany

Dieter Peitsch
dieter.peitsch@tu-berlin.de
Dept. of Aeronautics and Astronautics
Technische Universität Berlin
Berlin, Germany

Giuseppe Quaranta
giuseppe.quaranta@polimi.it
Dept. of Aerospace Science and Technology
Politecnico di Milano
Milan, Italy

ABSTRACT

Plasma actuators may be successfully employed as virtual control surfaces, located at the trailing edge of blades, both on the pressure and on the suction side, to control the aeroelastic response of a compressor cascade. Actuators generate an induced flow against the direction of the freestream. As a result, actuating on the pressure side yields an increase in lift and nose down pitching moment, whereas the opposite is obtained by operating on the suction side. A properly phased alternate pressure/suction side actuation allows to reduce vibration and to delay the flutter onset. This paper presents the development of a linear frequency domain reduced order model for lift and pitching moment of the plasma-equipped cascade. Specifically, an equivalent thin airfoil model is used as a physically consistent basis for the model. Modifications in the geometry of the thin airfoil are generated to account for the effective chord and camber changes induced by the plasma actuators, as well as for the effects of the neighboring blades. The model reproduces and predicts correctly the mean and the unsteady loads, along with the aerodynamic damping

*Address all correspondence to this author.

on the plasma equipped cascade. The relationship between the parameters of the reduced order model with the flow physics is highlighted.

INTRODUCTION

The quest for more efficient aero engines has significantly grown during the last few years. There is a high research effort to address the development of lighter engines, without degrading the overall delivered performance. An effective – largely pursued – solution would be to reduce the number of stages in compressors, whilst providing an unchanged total pressure ratio. To this aim, the pressure ratio per stage must be augmented, and this is achieved with highly cambered, long and light thin blades. However, these designs yield a dramatic increase in blade vibration and the narrowing of the flutter boundaries, together with an enhancement of separation phenomena and pressure losses. At the same time, also the aerodynamic performance is worsened, as separation phenomena – responsible of pressure losses – are intensified. A dramatic worsening of the aeroelastic and the aerodynamic performance of compressor blades is also encountered on pulsed detonation engines (PDE), widely investigated in turbomachinery research. These engines – potentially much more efficient than isobaric combustion engines – feature an isochoric combustion, which causes strong periodic pressure fluctuations impinging on the blades. Several solutions have been proposed to control flow separation and minimize pressure losses arising on these diverse configurations [1–8]. Among these solutions, plasma actuators seem to be very promising, thanks to their lightness and to their almost negligible intrusiveness in the flow. Moreover they feature very large bandwidth and do not suffer of performance degradation when operating under high temperatures and intense centrifugal force fields. A common dielectric barrier discharge plasma actuator consists of two electrodes separated by a dielectric material, see Fig. 1. One electrode is exposed to air, i.e. on the aerodynamic surface, and one is grounded within the dielectric material, inside the blade internal volume. When an alternate voltage is applied between the two electrodes, an electric discharge is initiated. The surrounding air is partially ionized, enabling a local modification of the flow momentum and, in turn, of the developed airloads.

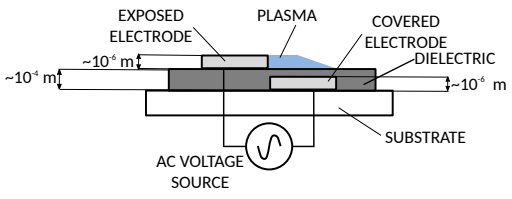

FIGURE 1: Schematic of a dielectric barrier discharge plasma actuator.

This kind of actuation has been proved to act effectively on separation, wake defect, and pressure losses on heavily loaded blades [9–11]. Differently from issues related to separation phenomena, the problem of controlling the structural and aeroelastic response of heavily loaded blades has not been extensively studied so far. Among the approaches proposed to control flutter on generic compressor blades, there are acoustic excitation [12, 13], zero-mean mass flow actuation [14–16] and piezo-actuation [17]. Though some promising results have been achieved, drawbacks of these concepts – some of which pointed out by the authors themselves in their works – may prevent their implementation on real engines. A novel concept of virtual control surfaces, realized with plasma actuators, has been proposed and assessed numerically by the authors in [18, 19]. This active control system aims to solve some of the aeroelastic feasibility problems encountered on heavily loaded compressor blades, and represents a step forward the realization of compressors at reduced number of stages. Specifically, in [18, 19] plasma actuators are modeled on the three central blades of the compressor cascade sketched in Fig. 2. The cascade – without actuation – reproduces the experimental rig of [20], with span-wise uniform NACA 65-series airfoils, a stagger angle of 43 deg. and a pitch to chord ratio of 0.75. Plasma actuators are

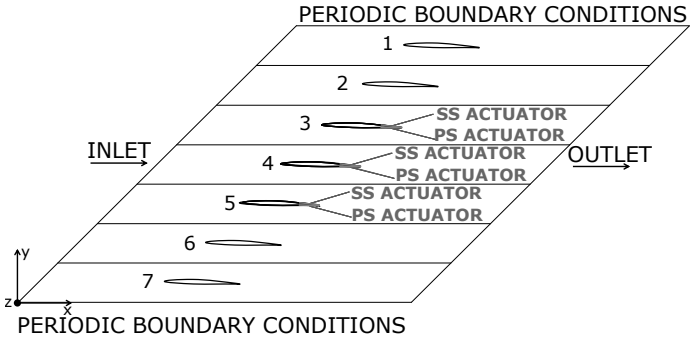

FIGURE 2: Schematic of the computational geometry for the compressor cascade, corresponding to the experimental rig of [20].

meant to be located at the trailing edge (TE) of the blades, both on the pressure and on the suction side (PS and SS), see Fig. 3.

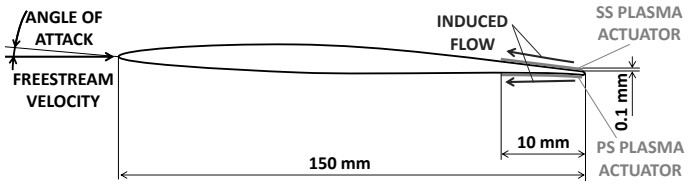

FIGURE 3: Sketch of the blade section with the plasma actuators.

Actuators are operated to generate an induced flow which is opposite to the direction of the freestream. This yields the

development of controlled recirculating flow areas, that cause a modification of the effective blade camber in a similar way to what is generated by the insertion of a Gurney Flap or a trailing edge spoiler [21]. Moreover, a shift of the Kutta condition application point downstream the physical TE is observed, consistently with what shown in [21]. Overall PS actuation has effects comparable to those achieved with a mechanical flap-like device. That is, lift and nose-down pitching moment are increased. On the contrary, SS actuation yields effects on the flow field which are analogous to those of mechanical spoilers. That is, lift and nose-down pitching moment are reduced [18, 19].

It's worth remarking that the present work is an exploratory investigation to assess whether plasma actuators could be suitable for load control in turbomachinery. The detailed design is planned for works to come and lies beyond the purposes of this manuscript. However, preliminary considerations on the practical implementation of plasma actuators on actual blades have been done. The actuators per se are very thin. The overall thickness of an actuator is expected to be $\sim 10^{-4}$ m see Ref. [10]. Therefore actuators could be installed also on quite thin trailing edges, by realizing appropriate cavities on the blade surface, both on the pressure and on the suction side. The first experimental studies envisaged in the near future will feature plasma actuators parallel to the chord and covering the whole span of the targeted linear cascade, see [20]. Successive studies will be be carried out on a rotating annulus, to investigate whether the transverse flow arising from the rotation requires to orient the actuators with a certain angle relative to the chord direction.

There are different possible approaches to fit the cables into the blades. The selected configuration depends on the geometrical arrangement of the actuators along the blade span. If the actuators will cover the entire span, the cables will be connected at the level of the blade root, where there will be less problems in terms of space. Dedicated cavities will be realized to locate the cables. When employing plasma actuators on the compressor rotor, the transmission of the signal from the fixed to the rotating frame will be realized by means of devices like those produced by Jordil Technic Sárl, which have already been used in [22] for a piezo-actuated aero engine blisk. An alternative, which would avoid the transmission of electrical signals from a fixed to a rotating system, was proposed by Iwrey in [23]. Iwrey suggested to exploit the rotation to generate the required voltage, by using electromagnetic effects. The concept of [23] is targeted to plasma actuators employed to control the tip clearance flow on gas turbine engines. Therefore, it is suitable also for the application of the present work. Iwrey proposed to locate one or more magnets on the casing of the engine and a magnet with a solenoid on each of the plasma actuated blades. The solenoid is connected to the electrodes of the plasma actuator. Due to the relative rotation of the blade and of the casing magnets, a voltage is generated on the solenoid. This voltage can indeed be used to feed the actuators, if an appropriate signal modulation is applied.

A further path, which is currently pursued by the authors in cooperation with the University of Salento, consists of developing micro controllers and micro generators, enough small to be located in targeted hollows, realized internally to the blades. In order to avoid a possible interference of the electrodes on the pressure side with those on the suction side, proper electromagnetic shielding will be employed between the two actuators. This shield can be realised by means of e.g. metal screens, foams or sheets.

The objective of this work is the development of a reduced order model (ROM) for the aerodynamic response of the plasma equipped cascade, assessed numerically in [18, 19]. The ROM is a powerful tool to perform large scale sensitivity studies and parametric optimizations, as well as to build up open- and closed-loop control architectures for the plasma actuation. It will be shown that the ROM allows for an accurate computation of the steady and unsteady airloads obtained on the cascade. Also the aerodynamic damping calculated with the model matches very well the values issued by Computational Fluid Dynamic (CFD) simulations. Because the ROM is conceived to reproduce the modifications in the blade mean line induced by plasma, it also provides a link with the near-body flow physics.

NUMERICAL SIMULATIONS

Plasma actuators are modeled numerically as local source terms to the flow momentum equations. The values of the forces per unit volume are taken from data of existing actuators and range from 50 to 900 mN/m. Further details on the numerical modeling of plasma actuators are given in [18, 19]. In these two works two-dimensional incompressible CFD assessments are performed with the finite volume solver Ansys CFX. Reynolds Averaged Navier Stokes equations, closed with the k – ω SST-Menter turbulence model, are employed. A multi-block structured grid composed of 550949 cells is realized. The reliability of the numerical results is checked by comparisons with experimental measurements and data from literature. More information on the set up and on the reliability checks of the unsteady simulations are reported in [18, 19] as well.

Computations with the blades at constant angle of attack – and actuation on the PS or on the SS – highlight a significant effect of plasma on the mean loads [18, 19]. PS actuation enables an increase in lift and nose-down pitching moment, whereas the opposite is achieved with SS actuation. At the same time, no remarkable drag rises are encountered on the actuated cascade. Steady state airloads with and without actuation, are displayed in Fig. 4.

Furthermore, time-resolved traveling wave mode simulations show the effectiveness of actuation on unsteady airloads and on the aerodynamic damping. During a traveling wave mode simulation, all blades oscillate at the same frequency and amplitude, but with a constant and uniform phasing, referred to as inter blade phase angle (IBPA) [24]. For these simulations, SS plasma is triggered during the upstroke phase – nose moving upward – of the pitching cycle. On the other hand, PS plasma is triggered during the downstroke phase. Figure 5 sketches the triggering of PS and SS actuation relative to the time history of the moment

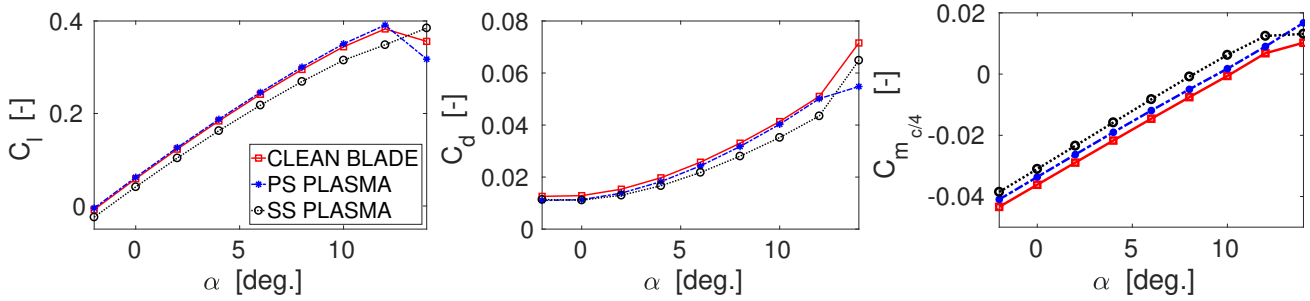

(a) Lift coefficient (b) Drag coefficient (c) Quarter-chord moment coefficient

FIGURE 4: Steady force coefficients versus the angle of attack for the clean central blade, together with the pressure or suction side actuated counterpart; PS: pressure side; SS: suction side; Re $\sim 3 \times 10^5$; plasma body force: 300 mN/m, both on PS and SS.

coefficient and to the blade motion. The light gray area highlights the operating window of the SS actuation. On the other hand, the dark gray area shows the operating window of the PS actuation.

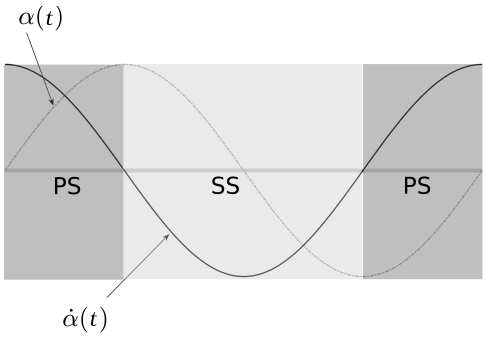

FIGURE 5: Sketch of PS and SS actuation triggering with respect to the blade motion $\alpha(t)$ and of its time derivative $\dot{\alpha}(t)$.

Figure 6 (top) shows TE details of the velocity magnitude field during an oscillation cycle of a traveling wave mode simulation. The velocity is made dimensionless with the freestream velocity. The central blade of the cascade is displayed. PS actuation generates the expected recirculating flow areas during the downstroke phase, with a consequent increase in the blade loading relative to the clean counterpart. The opposite occurs during the upstroke phase [18]. The oscillatory loads obtained with and without actuation are displayed in Fig. 6 (middle). The reduction in the unsteady lift and moment peaks enabled by alternate PS/SS actuation is clearly visible. Beneficial effects on the blade aeroelastic stability provided by unsteady plasma actuation are also obtained. Figure 6 (bottom) shows the non-dimensional aerodynamic work – defined as aerodynamic damping Ξ in [18] – versus the IBPA, with and without actuation.

With the ultimate aim of designing optimal open- and closed-loop control architectures, it is appears useful to develop a ROM for the plasma-equipped cascade, capable to predict accurately the unsteady loads of the blades. Furthermore, the availability of an accurate ROM may allow to extend significantly the parameter space for sensitivity analyses. In this way extensive studies of the aerodynamic/aeroelastic response to a wide range of geometrical and actuation parameters can be performed. In this work a linear frequency domain ROM is developed for the lift and the pitching moment of the plasma-equipped cascade. It is worth remarking that, being the angle of attack and the amplitude of oscillation small, it is possible to assume the aerodynamic response of the cascade as linear, at least as a first approximation. Moreover the flow is subsonic – consistently with [20, 25–27] – therefore nonlinearities arising from shocks or high gradients in the flow quantities are not present.

Notice that the derivation of a corresponding model for the clean cascade is straightforward, based on the counterpart with plasma actuations. Additionally, literature formulations which model the aerodynamic response of clean cascades, e.g. [28, 29], can be easily transposed to the present model. Therefore the attention is focused here on a model for the plasma-equipped cascade without plasma actuators. The proposed ROM is also easily extensible to any active control system inducing a modification in the effective camber of the blade, which is the main effect of the plasma actuators proposed here.

Because the effects of alternate PS/SS actuation are comparable to those of a flap-like device downward/upward deflected [18, 19], an equivalent three-segments thin line is used as a basis for the ROM. Indeed this approach is consistent with that adopted in [21, 30] for an helicopter blade section equipped with a trailing edge flap-like device deflected harmonically. The first segment is meant to reproduce the contribution of the blade to the airloads. The second segment is representative of the effects of modification in the effective blade shape, due to plasma actuation. The third segment, interpreted as a trim tab, is meant to reproduce the downstream shift of the Kutta condition application point due to plasma, as well as the contribution to airloads induced by the neighboring blades. According to the IBPA, the effects of the neighboring blades on a generic blade of the cascade can be nozzle-equivalent or diffuser-equivalent [31] – i.e the effective

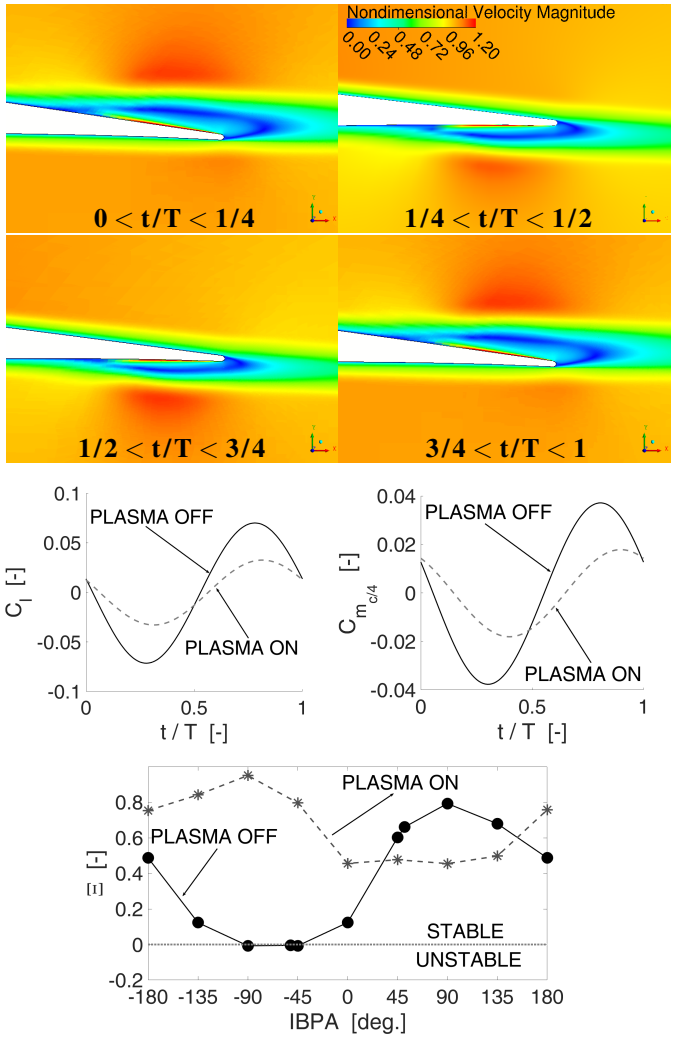

FIGURE 6: Top: TE detail of velocity magnitude, normalized by the freestream velocity, over the oscillation cycle; plasma actuation on. Middle: time history of lift and moment coefficient oscillations without and with actuation. Bottom: aerodynamic damping versus IBPA with and without plasma. Re $\sim 1.9\times10^5$; IBPA = -51.43 deg.; $\alpha = 2+\sin 2\pi ft+4\times \mathrm{IBPA}\pi/180$ deg.; $f = 19.17$ Hz, $T = 1/f$; PS body force: 225 mN/m; SS body force: 450 mN/m.

incidence is enhanced or reduced – therefore increasing or decreasing the aerodynamic loading. The same approach is adopted to model the static lift and moment enhancements/reductions, as due to an equivalent camber/chord modification effect. It is shown that, with few parameters, it is possible to reproduce accurately the steady and the unsteady loads on the plasma-equipped cascade in design and off design conditions. The model appears capable to work reasonably in a predictive manner, in computing airloads for arbitrary values of the body force or of the IBPA. Also the aerodynamic damping, which is a widely used parameter to estimate the aeroelastic stability of a cascade [32], is reproduced correctly by the ROM. Moreover, especially at low-to-moderate reduced frequencies, the ROM allows to get an idea of the actuation effects on the near blade flow fields.

ANALYTICAL FORMULATION OF THE REDUCED ORDER MODEL

The analytical reduced order model developed in this work has its cornerstone in theory of Küssner-Schwarz (KS) [33, 34]. This approach has already been successfully employed to reproduce the unsteady loads generated by a flap-like device on a helicopter blade section [21, 30]. The fundamental theory uses a thin-airfoil approach, with the assumptions of:

- potential fluid flow
- incompressible flow
- linear flow response

These assumptions are valid for the simulated conditions, being the blade angle of attack and oscillation amplitude both small. Moreover the flow is subsonic and no separation phenomena are present. These conditions are in agreement with the investigations performed on linear compressors in [20, 25–27]. The model of Verdon [35], which is one of the most referenced reduced models for turbomachinery bladings – without active control –, is linear and widely used for aeroelasticity problems. It's also worth remarking that plasma actuators are employed here for two purposes: i) control of vibration; ii) enlargement of flutter boundaries. Small angles of attack are certainly suitable for vibration problems and for most of the flutter problems. The ROM proposed here is not valid for stall flutter phenomena. By the way the plasma actuation proposed here and in Refs. [18, 19] is not addressed toward stall flutter. The problem of stall flutter has to be tackled by counteracting stall – detrimental first of all for the aerodynamic performance – and not the consequent flutter. The present arrangement of plasma actuators is not targeted to control stall. For this phenomenon, actuators should be placed much closer to the leading edge on the suction side (or even on the engine casing) and should feature induced flow directed downstream, see e.g. [9–11]. The proposed model can be easily made suitable for transonic flows by using the approach proposed in [36, chapter 8]. In accordance with the small perturbation hypothesis, the aerodynamic solution of the unsteady flow around an airfoil can be obtained as a linear combination of elementary solutions. These latter correspond to the separate effects of angle of attack, camber and thickness distribution – see [33, 37, 38]. Notice that also the effect of the neighboring blades of the cascade can be reduced to a modification of the effective camber and chord of the blade section, at least for low-to-moderate reduced frequencies. Indeed, according to the IBPA, the effect of a neighboring blade on a reference blade can be either an acceleration or a deceleration of the flow, relative to the flow of an isolated airfoil. If the flow under the blade is accelerated, then lift and moment are reduced, whereas the opposite occurs if the flow is decelerated. Complementary effects are encountered when the flow above the blade is accelerated or decelerated. In general the neighboring blades

modify the effective incidence of the blade – compared to the isolated airfoil – as if the section would feature a different chord and camber. As a result, the proposed ROM, conceived to be applied to an isolated airfoil in [21], can be extended to a linear cascade, as the one under consideration. The KS formulation allows for a quick and accurate computation of the pressure distribution – in terms of differences between the lower and the upper side – for an arbitrarily shaped mean line affected by any kind of motion, as far as the assumption of small perturbations is valid. The capability of the KS model to deal with any kind of motion, comes directly from theoretical foundation of the model. Because it is based on the Fourier decomposition of the velocity distribution along the mean line, then a lifting section – cascade or isolated airfoil – moves according to the generic harmonic law:

$$z(x,t) = |\tilde{z}(\omega,x)|\mathrm{e}^{(\mathrm{j}\omega t+\varphi_z(\omega,x))}, \tag{1}$$

where $\tilde{(\cdot)}$ is the symbol used for the Fourier transformed variables and φ_z represents the phase of $\tilde{z}$. The parameter $\omega = 2\pi \mathrm{f}$ is the circular frequency of the harmonic motion – being f the frequency in Hz. The upwash velocity from the airfoil motion can be computed as follows:

$$v(x,t) = \frac{Dz}{Dt} = \frac{\partial z}{\partial t} + \frac{\partial z}{\partial x}\frac{\partial x}{\partial t} = \frac{\partial z}{\partial t} + U\frac{\partial z}{\partial x}. \tag{2}$$

The Fourier series of the spatial velocity distribution allows for the computation of the upwash coefficients P_0, ...P_n, i.e.,

$$v(\theta,t) = g(\theta)\mathrm{e}^{(\mathrm{j}\omega t+\varphi(\theta))} = -U\mathrm{e}^{\mathrm{j}\omega t}\left(P_0 + 2\sum_{n=1}^{\infty} P_n \cos n\theta\right), \tag{3}$$

where θ is an angular abscissa that corresponds to the position x along the airfoil chord, through the classical transformation $x = b\cos\theta$, being $2b$ the chord of the airfoil. The upwash coefficients are:

$$P_n = -\frac{1}{U\pi}\int_0^{\pi} g(\theta)\mathrm{e}^{\mathrm{j}\varphi(\theta)}\cos n\theta \mathrm{d}\theta \tag{4}$$

Küssner and Schwarz [33, 34] proved that the difference of pressure coefficient between pressure and suction side can be expressed as a Fourier series:

$$\Delta \mathrm{C_P}(\theta,t) = \mathrm{e}^{\mathrm{j}\omega t}\left(4A_o\tan\frac{\theta}{2} + 8\sum_{n=1}^{\infty} A_n \sin n\theta\right), \tag{5}$$

with the A_n coefficients that can be written as function of the upwash coefficients, i.e.,

$$A_0 = C(k)\,(P_0 + P_1) - P_1 \tag{6}$$

$$A_n = P_n + \frac{\mathrm{j}k}{2n}\,(P_{n-1} - P_{n+1}) \qquad \forall n > 0 \tag{7}$$

In Eqs. 7 k is the reduced frequency $k = \frac{\omega b}{U}$ and $C(k)$ is the Theodorsen's function [37]. The aerodynamic lift $\mathrm{L}(t)$ and pitching moment $\mathrm{M_0}(t)$ are obtained by the integration of the difference of pressure along the mean line:

$$\mathrm{L}(t) = \frac{1}{2}\rho U^2 b\int_0^{\pi} \Delta \mathrm{C_P}(\theta,t)\sin\theta \mathrm{d}\theta \tag{8}$$

$$\mathrm{M_0}(t) = -\frac{1}{2}\rho U^2 b^2\int_0^{\pi} (\cos\theta - \hat{x}_0)\,\Delta \mathrm{C_P}(\theta,t)\sin\theta \mathrm{d}\theta \tag{9}$$

where the moment is computed with respect to the point $\hat{x}_0 = x_0/b$. For pitch and plunge harmonic motions, the KS theory leads to results that are equivalent to the classical Theodorsen's theory [34]. The development of the present ROM starts from the definition of a parametric formulation based on the KS theory. A numerical optimization is then performed, to identify the appropriate values of the parameters through a comparison with CFD data. Exploiting an approach similar to the one used in [21, 39], the blade is represented by a piecewise-linear thin-line airfoil composed by a fixed part plus two virtual movable surfaces: a flap and a trim tab, see Fig. 7. The second segment models the effects of the plasma actuation – equivalent to a flap-like device deflected upward/downward – on the blade. The last segment takes into account two phenomena: i) the shift of the Kutta condition downstream the physical TE, caused by the actuation, and the effect of the neighboring blades, which can either increase or decrease the actual incidence, according to the IBPA. In the following, the first segment of the piecewise mean line will be referred to as Equivalent Blade (EB), the second segment as Plasma-Equivalent Flap (PEF) and the third segment as Equivalent Trim Tab (ETT). The geometrical and motion parameters considered for the model

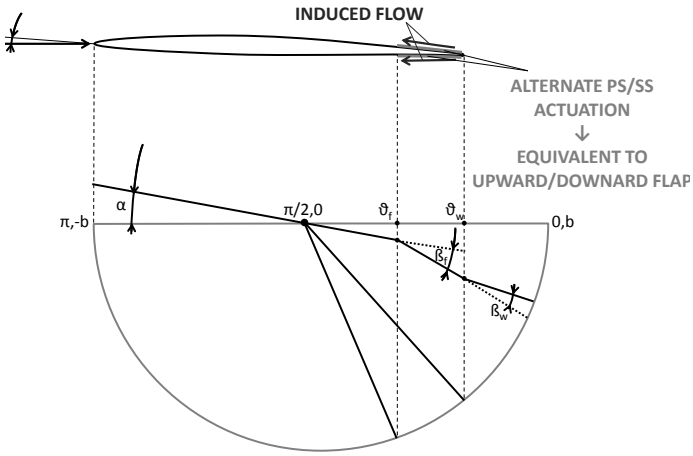

FIGURE 7: Sketch of the blade section with plasma actuators, together with the equivalent thin-line geometry.

order reduction are given in Fig. 7. The parameter $\alpha \in \mathbb{C}$ represents the oscillating motion of the EB about the mid chord $c/2$ of

the virtual flat-plate thin-line geometry. Again, those oscillations can be physically interpreted as local camber variation for the thin-line airfoil. The parameter x_f indicates the starting point of PEF along the chord of the equivalent KS model, and it can be also expressed through the angle $\theta_f = \arccos(x_f/b)$. The parameter x_c, and the corresponding angle $\theta_c = \arccos(x_c/b)$, indicate the TE of the physical airfoil along the chord of the virtual thin-line airfoil geometry. The complex parameter $\beta_f \in \mathbb{C}$ represents the amplitude and phase of the PEF rotation relative to the EB, whereas $\beta_w \in \mathbb{C}$ represents the amplitude and phase of the ETT rotation with respect to the PEF. All of the geometrical parameters of the KS model are expressed as non-dimensional, using the thin airfoil chord $c_k = 2b$ as the reference quantity. The position θ_w represents the fact the virtual thin-plate airfoil representation should have a longer chord than the physical airfoil, because the point where the Kutta condition must be enforced is not at the airfoil TE. However, to compute the correctly scaled lift and moment, the pressure coefficient in the virtual thin-plate model is integrated from the leading edge to θ_w, because the last portion of the virtual airfoil model is only virtual and does not correspond to a physical surface that can carry loads.

A generic plasma equipped blade of the cascade is modeled as a linear system with three degrees of freedom. These are: the pitch of the blade, the plunge of the blade and the oscillation of a plasma-equivalent flap, i.e. the alternate PS/SS actuation. According to the assumption of linearity of the model, it is possible to study the system response in terms of aerodynamic loads for each of the three aforementioned forcing motions, separately. Furthermore, the upwash velocity can be expressed as:

$$v = v_{\alpha_0}(x) + v_\alpha(x,t) + v_h(x,t) + v_{\beta_0}(x) + v_\beta(x,t) \tag{10}$$

where the subscript α represents the velocity terms associated to the pitch motion, the subscript h indicates the velocity terms issued from the plunge motion and the subscript β is related to the velocity terms from the plasma-equivalent flap motion. The velocity contributions related to each of the degrees of freedom can be split into a steady term and a time dependent term, representative of the steady mean value and of harmonic oscillation, respectively. Accordingly, the aerodynamic forces can be written as:

$$F_a = F_{\alpha_0}(x) + F_\alpha(x,t) + F_h(x,t) + F_{\beta_0}(x) + F_\beta(x,t) \tag{11}$$

In the present work pitch oscillations are considered with zero mean value, hence $v_{\alpha_0}(x) = 0$ in Eq. (10) and therefore $F_{\alpha_0}(x) = 0$ in Eq. (11). The model order reduction is performed for the terms of Eqs. (10),(11) with subscript α, β_0 and β. The plunge motion of the blades is not considered in this work and is left as a further outlook. Indeed the blade bending stiffness is much larger than the torsional counterpart, for the cascade under consideration [20, 27]. Moreover, the experimental results of [26] showed that the torsional mode is the most critical for this cascade. The analysis to compute the unsteady loads due to pitch and plunge motion is not reported here, because it is equivalent to the standard approach presented in Ref. [34, Chapter 13]. For the computation of the lift and moment associated to EB, PEF and ETT rotations, the equivalent geometry for the ROM takes the following mathematical form :

$$z(x,t) = \begin{cases} (x - x_{c/2})\tilde{\alpha}e^{j\omega t} & \text{if} \quad x \le x_f \\ (x - x_{c/2})\tilde{\alpha}e^{j\omega t} - (x - x_f)\tilde{\beta}_f e^{j\omega t} & \text{if} \quad x_f < x \le x_w \\ (x - x_{c/2})\tilde{\alpha}e^{j\omega t} - (x - x_f)\tilde{\beta}_f e^{j\omega t} + & \\ -(x - x_c)\tilde{\beta}_w e^{j\omega t} & \text{if} \quad x > x_w. \end{cases} \tag{12}$$

Notice that the blades oscillate about the mid-chord $x_{c/2}$ both in the CFD and in the ROM geometry. The upwash velocity is computed according to Eq. (2) and expressed as a function of θ. The employment of relative rotations as degrees of freedom allows to build an incremental model for the lift and moment. Consider initially the upwash coefficients and the aerodynamic loads for the PEF, extending from θ_f to θ_w, oscillating with respect to its initial point θ_f, see Fig. 7. The vertical displacement $z(x,t)$ of the PEF is:

$$z(x,t) = -(x - x_f)\tilde{\beta}_f e^{j\omega t}, \quad x_f < x < x_c \tag{13}$$

where $\tilde{\beta}_f \in \mathbb{C}$ is a complex parameter representing the Fourier transformation of the PEF rotation at circular frequency ω. The vertical perturbation velocity is:

$$\begin{aligned} v(\theta,t) &= -U\left(jk\left(\cos\theta - \bar{x}_f\right) + 1\right)\tilde{\beta}_f e^{j\omega t} \\ &= g_v(\theta)e^{j\omega t}, \quad \theta_c < \theta < \theta_f \end{aligned} \tag{14}$$

with $\bar{x}_f = x_f/b$. The upwash coefficients P_n are then computed through the Fourier transformation of the vertical perturbation velocity, within the interval $[\theta_w \quad \theta_f]$, see [21]:

$$P_n = -\frac{\tilde{\beta}_f}{U\pi}\int_{\theta_w}^{\theta_f} g(\theta)e^{j\varphi(\theta)}\cos n\theta \, d\theta \tag{15}$$

The series of P_n is convergent toward zero, so it can be truncated after N terms, where N is selected as the first coefficient where the order of magnitude is three times smaller than the leading term of the series. The A_n coefficients are computed using Eqs. (7). Similarly, the computation of ΔC_P through Eq. (5) is straightforward. The aerodynamic loads can be obtained by substituting the resulting expression of ΔC_P in Eqs. (9) and integrating the ΔC_P between the leading edge and the TE at θ_w, i.e.,

$$C_l = \frac{1}{2}\int_{\theta_w}^{\pi}\left(4A_0\tan\frac{\theta}{2} + 8\sum_{n=1}^{N}A_n\sin n\theta\right)\sin\theta \, d\theta \tag{16}$$

The moment coefficient related to the mid-chord is

$$C_m = -\frac{1}{4}\int_{\theta_w}^{\pi}\left(4A_0\tan\frac{\theta}{2}+8\sum_{n=1}^{N}A_n\sin n\theta\right)\sin\theta\cos\theta d\theta \quad (17)$$

An identical approach can be used to compute the lift and moment coefficients from the rotation of the ETT.

CFD results, better detailed in [18, 19], are used as a reference basis for the computations of the ROM parameters. First numerical results obtained on the cascade with blades fixed at zero angle of attack are considered. Configurations with constant PS or SS actuation are employed. Several values of the plasma body force – ranging from 50 to 900 mN/m – are taken into account. This allows to assess the sensitivity of the ROM parameters to the actuation intensity. An interpolation of the ROM parameters over the actuation is performed. Then the predictive capabilities of the model are checked for an arbitrary value of the body force, both for the PS and for the SS actuation. Subsequently, traveling wave pitch mode simulations – with reduced frequencies of $k = 2\pi fc/2U_\infty$ of 0.0720 and 0.2299 for several IBPAs ranging from -180 to 180 deg. – are used. This allows for estimating the sensitivity of the model parameters to the IBPA. An alternate PS/SS actuation during the blade pitching cycle is used. The PS body force – triggered during the blade downstroke phase – is kept to 225 mN/m. The SS body force – activated during the blade upstroke phase – is set to 450 mN/m, see [18].

The ROM is determined by means of an optimization procedure performed at a fixed IBPAs, first for off design and then for design conditions. The objective of the optimization is the minimization of the error between the CFD-computed lift and moment coefficients and the corresponding quantities computed with the KS model of Fig. 7. One fitting is carried out on the results at constant angle of attack, and another fitting is performed for traveling wave mode simulations. The airloads achieved with the two fitting procedures can be superimposed. This can be useful when – within a traveling wave motion – the mean angle of attack or body force are non-zero. A least squares-based optimization algorithm is used for the minimization procedure. In particular, the function to be minimized is written as follows:

$$\begin{aligned} F(\mathbf{p}) = &\frac{1}{\Re(C_{l_{NUM}})^2}\Re(C_{l_{NUM}}-C_{l_K}(\mathbf{p}))^2 \quad + \quad (18)\\ &+\frac{1}{\Im(C_{l_{NUM}})^2}\Im(C_{l_{NUM}}-C_{l_K}(\mathbf{p}))^2 \quad +\\ &+\frac{1}{\Re(C_{m_{NUM}})^2}\Re(C_{m_{NUM}}-C_{m_K}(\mathbf{p}))^2 +\\ &+\frac{1}{\Im(C_{m_{NUM}})^2}\Im(C_{m_{NUM}}-C_{m_K}(\mathbf{p}))^2 \end{aligned}$$

where $C_{l_{NUM}}$ and $C_{m_{NUM}}$ are the lift and moment coefficients computed from the CFD simulations. The array $\mathbf{p}$ contains the geometrical and motion free parameters of the KS model discussed above, see also Fig. 7, i.e. $\mathbf{p} = \{\theta_w, \theta_f, \tilde{\beta}_f, \tilde{\beta}_w\}$, and it is composed of six independent quantities. $C_{l_K}(\mathbf{p})$ and $C_{m_K}(\mathbf{p})$ are the KS aerodynamic loads to be computed by the optimization algorithm according to the free parameters in $\mathbf{p}$. Notice that for the computations with the blades at constant angle of attack, the airloads, as well as the parameters $\mathbf{p}$, are real quantities. Moreover different sets of free parameters are selected – among all those of the KS formulation – for the fitting at constant angle of attack or in traveling wave mode conditions. A multistart approach is used for the minimization, to avoid the identification of a local minimum that does not correspond to the global one. Additionally, to achieve physically consistent solutions, constraints are imposed a priori to the free parameters.

REDUCED ORDER MODEL FOR BLADES AT CONSTANT ANGLE OF ATTACK

In this section the ROM for the blades at zero angle of attack, with PS or SS actuation is developed. It is worth recalling that PS plasma yields effects which are comparable to those of a flap-like device deflected downward. On the other hand, SS plasma acts similarly to of a flap-like device deflected upward. Additionally, due to the actuation, the Kutta condition is shifted downstream, see also [21], and the neighboring blades provide further modifications in the effective angle of attack, i.e in the blade camber and chord. Because both the actuation and the plasma body force are constant, the parameters $\mathbf{p}$ of the ROM are real quantities. For the minimization of Eq. (18) – without imaginary terms – the length of the PEF, determined by the parameter θ_f, is fixed to the value of the CFD model. Namely the length of the PEF is defined to cover the same chord-percentage of the numerical counterpart. The length of the ETT – defined by the parameter θ_w – is fixed to 1% of the chord. This value is issued from evaluations of the average shift of the Kutta condition points for the different body forces – on PS and SS, respectively. The estimation is valid for blades at constant angle of attack and with body force always switched on during the simulation. The location of this point is estimated as the first intersecting point of the streamlines coming out of the PS and of those coming out of the SS [21]. The deflection amplitude of the PEF and of the ETT, β_f and β_w respectively, are left as free parameters for the optimization. Constraints are imposed to the free parameters in order to ensure the achievement of a physically consistent solution. The angle of attack of the EB is set to 0 degrees.

Figures 8a and 8b show the amplitudes of the PEF and of the ETT, β_f and β_w respectively, obtained with the optimization procedure at different body forces both on the PS and on the SS. The parameter β_f ranges between 0 and 0.2 deg. and β_w lies between -0.2 and -0.45 degrees. For the PS actuation β_f ranges between -0.1 and -0.5 whereas β_w varies between -0.1 and -0.5 degrees. Figures 8c,8d show the lift and mid-chord moment coefficients computed with the ROM, together with the counterpart resulting from CFD computations. Again, different body forces are shown,

Airloads	C_l	$C_{m_{c/2}}$
CFD	0.0472	-0.0208
ROM	0.0475	-0.0209
$\Delta\%$	0.6373	-0.2886

(a) PS Actuation

Airloads	C_l	$C_{m_{c/2}}$
CFD	0.0619	-0.0193
ROM	0.0613	-0.0193
$\Delta\%$	0.9979	-0.0901

(b) SS Actuation

TABLE 1: Lift and mid chord moment coefficients resulting from interpolating the ROM and achieved with CFD computations performed a posteriori; angle of attack: 0 deg.; Re $\sim 3\times10^5$; plasma body force: 300 mN/m, both on PS and SS.

both for PS and SS actuation. The ROM is found to capture very well the two force coefficients at each of the body forces taken under consideration. In order to assess the predictive capabilities of the ROM, the force coefficients of Figs. 8c,8d are interpolated for arbitrary values of the body forces. The obtained quantities are compared to the counterparts achieved with numerical computations performed a posteriori. Table 1 shows the comparison of the lift and moment coefficient obtained by interpolating the ROM at body force of 225 mN/m, together with the CFD results achieved a posteriori. The percent difference between CFD and ROM is always below 1%, showing that the ROM is capable to operate correctly also in a predictive manner. This is very useful, because the ROM can indeed be successfully used to perform sensitivity studies, reducing drastically the computational burden.

REDUCED ORDER MODEL FOR BLADES IN TRAVELING WAVE PITCH MODE

In this section the ROM is derived for the blades featuring a traveling wave pitch mode. The flow and motion conditions are the same of [18, 19]. The blades oscillate in pitch with amplitude of 1 deg., about a mean angle of 2 deg. Notice that in this section the ROM is developed only for the oscillating part of the motion and of the airloads. In fact, because plasma is operated in un unsteady manner with zero mean body force, there is no effect of actuation on the mean loads in this case. The steady mean contribution can be easily added by using the thin-line formulas. For instance, the steady lift can be computed directly as $2\pi(\alpha-\alpha_0)$, being α_0 the zero-lift angle, see [40, Chapter 5]. The parameters of the ROM are obtained by performing the minimization of Eq. (18) at several IBPAs in the range [-180 180] degrees. Consistently with the alternate PS/SS actuation and to the oscillating motion of the blades, the PEF and the ETT are assumed to feature an harmonic motion, at the same frequency of the blade, but with different phase. The ROM is first developed for off-design conditions [20, 27] and then for the design conditions investigated in [20, 25]. The results obtained in off design conditions are presented first because they are indeed those under which plasma actuators are meant to operate, and therefore the most significant to be reproduced.

The free parameters $\mathbf{p}$ for the optimization algorithm are the amplitude of the PEF and of the ETT, alongside the phase and length of the ETT. Therefore four parameters have to be computed in total. The length of the PEF is kept to the same value imposed in the previous section. That is the EF is assumed to cover the same chord percentage of the numerical plasma. Analogously, the phase of the PEF is kept at the same value of the numerical model, i.e., $+\pi/2$ relative to the motion of the EB. The amplitude and phase of the EB, are kept equal to those of the numerical model. Because here the fitting is performed on the central blade of the cascade, its oscillation phase corresponds to $4\times$ IBPA. The real and the imaginary part of lift and moment coefficients issued by CFD computations are used as a reference to minimize Eq. (18).

Figures 9a,9b,9c,9d show the geometrical parameters of the ROM achieved at four IBPAs for the off design conditions. Because the cascade is close to the instability [20, 27] the computed parameters exhibit a highly oscillating behavior with respect to the IBPA. Indeed the equivalent geometry has to generate airloads which exhibit large excursions with the IBPA. The deflection amplitudes of the PEF and of the ETT span approximately from -50 to 50 deg., whereas the phase of the ETT ranges between approximately -180 and 180 degrees. The length of the ETT is also depicted, and defined as the percent enlargement of the chord relative to the physical TE. This parameter is indicated as x_w and is related to θ_w by the following expression [21]:

$$x_w = 1 + \frac{1-\cos\theta_w}{1+\cos\theta_w} \tag{19}$$

This quantity is bounded within a narrower range and is always smaller than 2% of the chord. Notice that the values of the ROM parameters computed at -180 deg. and at 180 deg. are the same. It is appropriate to remark that the oscillations found for the PEF and and for the ET are quite high to be considered as deflections of trailing edge control surfaces, and exhibit a remarkable oscillatory behaviour with respect to the IBPA. This is probably due to the fact that, at moderate-to-high reduced frequencies, like the one under consideration, the wave length of the pressure wave associated to the IBPAs gets closer to the wave length related to the blade oscillation. Therefore the effects of the neighboring blades interfere more on the aerodynamic response of the blade, compared to the case of lower reduced frequencies. As a result the ROM is capable to calculate accurately the unsteady airloads, but it loses slightly in physical meaningfulness. In these conditions more degrees of freedom, related to the mutual effects of the blades should be involved, to achieve a more realistic consistency with the physics. One possibility could be to try to consider multiple thin-line geometries disposed in cascade, e.g. with an approach similar to [28, 35]. A multi-blade model is currently under study and will be the focus of future works.

Figure 10 shows the numerical near body flow field of the vorticity – made dimensionless by the ratio of chord over freestream

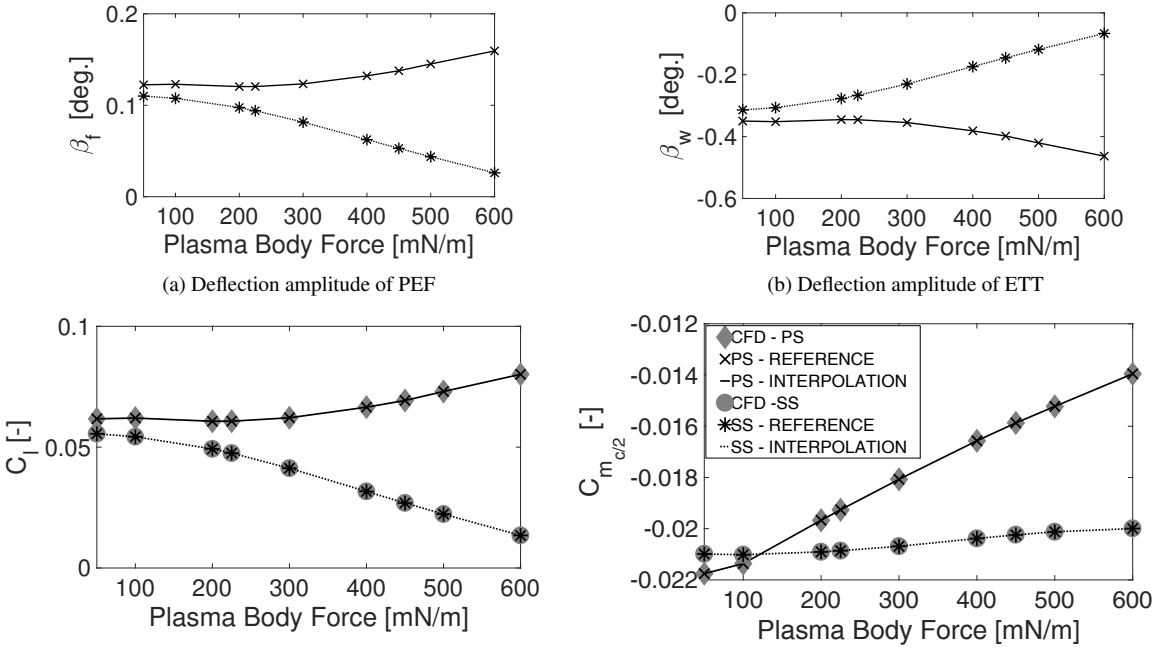

(a) Deflection amplitude of PEF

(b) Deflection amplitude of ETT

(c) Lift coefficient

(d) Mid-chord moment coefficient

FIGURE 8: Top: parameters of the equivalent geometry. Bottom: force coefficients coefficients obtained with the fitting over the CFD data versus the plasma body force. Re $\sim 3 \times 10^5$; $\alpha = 0$ deg.;plasma body force: 300 mN/m, both on PS and SS.

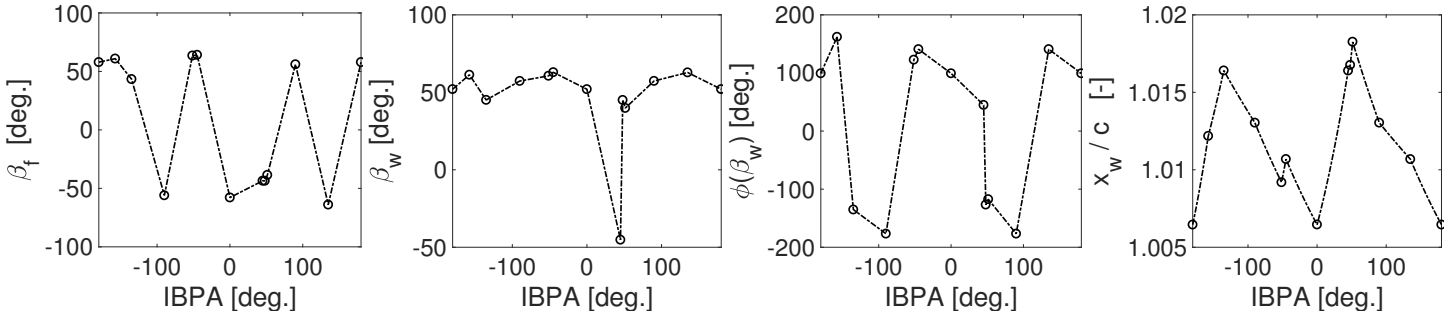

(a) Deflection amplitude of PEF

(b) Deflection amplitude of ETT

(c) Phase angle of ETT

(d) Lenght of ETT

FIGURE 9: Parameters of the ROM equivalent geometry; off design conditions; k = 0.2299; Re $\sim 1.6 \times 10^5$; PS plasma body force: 225 mN/m; SS body force: 450 mN/m.

velocity – at IBPA = -51.43 degrees. Four time steps of the pitch oscillating cycle are displayed, and the alternate PS/SS plasma actuation is clearly visible. Indeed the positive and negative peaks of vorticity in the TE area are related to the recirculating flow regions associated to PS/SS actuation. The central blade is depicted. The thin line geometry issued by the ROM is plotted over the numerical flow field. The three segments of the equivalent geometry are displayed as a black piece-wise line. The ROM equivalent geometry follows the motion of the blades and reproduces the camber modifications related to the alternate PS/SS actuation. Namely, the PEF is deflected upward when SS actuation is triggered. Consistently, the PEF is deflected downward during the operating cycle of the PS actuator. Finally the ETT accounts for the combined effects of the neighboring blades and of the plasma-induced chord enlargement.

Figure 11 shows the hysteresis loops of lift and mid-chord moment coefficients obtained with the ROM and with CFD computations on the cascade with alternate PS/SS actuation. Namely, the first positive and negative nodal diameters of an annulus equivalent to the linear cascade are displayed. The value IBPA = -51.43 deg. is close to the aeroelastic instability threshold of the cascade, detected numerically [20] and experimentally [27] at

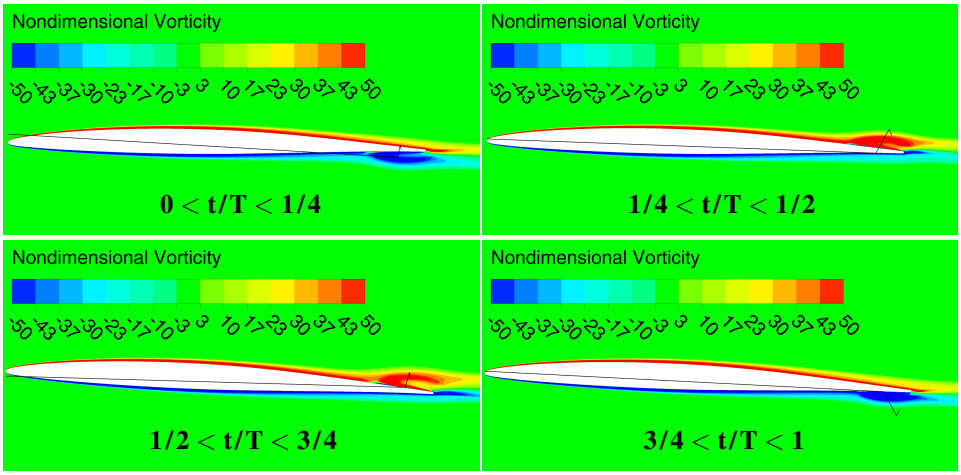

FIGURE 10: Non dimensional vorticity field for the central blade of the cascade with alternate PS/SS actuation, together with the equivalent geometry computed with the ROM; off design conditions; k = 0.2299; Re $\sim 1.6 \times 10^5$; oscillation amplitude: 1 deg.; PS plasma body force: 225 mN/m; SS body force: 450 mN/m.

this reduced frequency ($k = 0.2299$). A very good agreement between the ROM and the CFD is found for the two IBPAs both in terms of lift and moment coefficients. The same accuracy is obtained with all of the remaining IBPAs on which the ROM has been computed. The actuators are conceived to act primarily on the aeroelastic response of the cascade. Therefore it appears useful to highlight the capability of the ROM in predicting the aerodynamic work of the blades. This quantity defines the energy exchange between the flow and the blades. When the flow feeds the blade with energy, then the aeroelastic response gets unstable and flutter can occur. The aerodynamic damping is a dimensionless expression of the aerodynamic work. Consistently with [32], the aerodynamic damping Ξ is here computed as:

$$\Xi = -\Im C_m. \tag{20}$$

Table 2 shows the percent difference between the values of Ξ issued from CFD and the counterparts achieved with the ROM. The percent difference is smaller than 3.2% for all of the IBPAs considered, showing how the ROM is reliable also for evaluating the aeroelastic stability of the cascade.

By applying the procedure adopted in the previous section, it is possible to employ the ROM in a predictive manner. This allows for computing the unsteady lift and moment coefficients for an arbitrary IBPA, without the need of CFD computations. It is found that the ROM can be indeed used in a predictive manner, also for traveling wave mode simulations. Figure 12 is an example of the lift and moment hysteresis curves predicted by interpolation of the ROM parameters, against CFD results obtained a posteriori. The displayed IBPA corresponds to 112.5 deg. Actually, the remarkably oscillating behavior obtained for the ROM parameters depicted in Fig. 9 does not allow to get excellent predictions for all of the IBPAs. The one shown in Fig. 12 is one of the best matching obtained with the employment of the ROM in a predictive manner. An good agreement between CFD and ROM is observed. The ROM is found capable to predict correctly also the near-body flow physics, similarly to what shown in Fig. 10. The results are not reported here for brevity purposes.

The ROM is computed also for operating design conditions of the cascade. Specifically, the oscillation amplitude is 1 deg. and the semi-chord-based reduced frequency is 0.0720. The body force is again 225 mN/m on the PS and 450 mN/m on the SS. Figures 13a,13b,13c,13c shows the ROM geometrical parameters achieved in these conditions at IBPA = [-180, -90, 90, 180] deg. The parameters computed at IBPA = -180 deg. are again the same of the counterparts obtained at IBPA = 180 deg. The deflection amplitudes of the PEF and of the ETT range approximately between -6 and 3 degrees. The phase of the ETT spans from approximately -110 and -90 degrees. That is the ETT is in lag relative the PEF.

It is found that the effective chord length increase of the PEF is below 1% of the chord, i.e, slightly lower than the steady state counterpart at body force of 225 and 450 mN/m. This effect balances somehow the fact that the deflection amplitudes of the PEF and of the ETT are larger than the values obtained at constant angle of attack for body forces in the range [225 and 450] mN/m. These differences show that, for the blades oscillating in traveling wave, the camber modifications induced by the actuation are more relevant than the chord enlargement effects induced by the shift of the Kutta condition and by the influence of the neighboring blades. In general, lower absolute values of the PEF and ETT deflections angles are found with respect to the off design conditions. This is somehow expected, because for growing reduced frequencies – above the value of the phase inversion – the amplitude of the unsteady loads results larger, see [38]. Additionally, the phase of the ETT is always negative, whereas, for the off design conditions

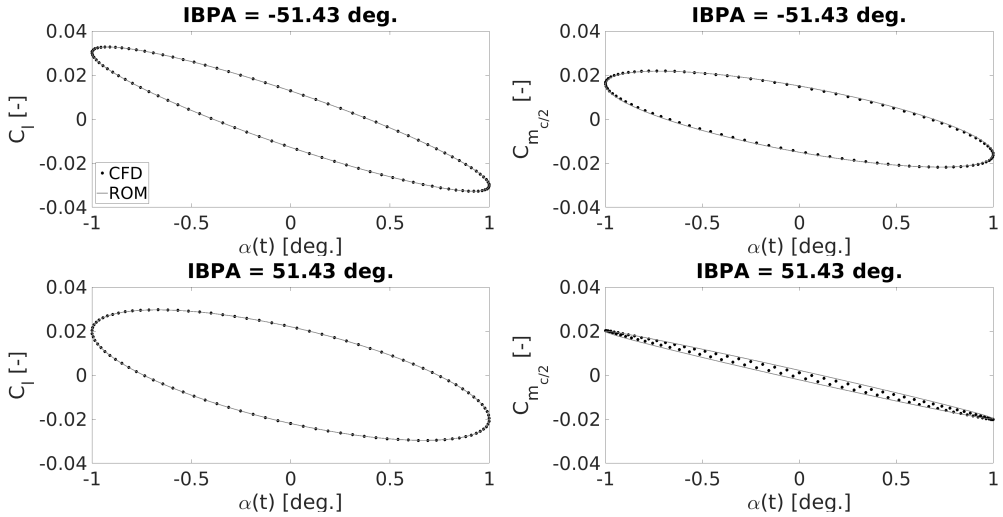

FIGURE 11: Hysteresis curves of lift and moment coefficient for the central blade of the cascade with alternate PS/SS actuation, together with the counterpart of the ROM; off design conditions; Re $\sim 1.9 \times 10^5$; PS plasma body force: 225 mN/m; SS body force: 450 mN/m.

IBPA [deg.]	-180	-157.5	-135	-90	-51.43	-45	0	45	48	51.43	90	135	180
$\Delta\Xi_{\mathbf{CFD,ROM}}\%$	0.71	3.86	2.15	1.97	2.25	2.27	0.78	0.63	0.91	1.24	2.21	3.18	0.71

TABLE 2: Percent difference of aerodynamic damping computing with CFD and with the ROM. Central blade of the cascade with alternate PS/SS actuation; off design conditions; Re $\sim 1.9 \times 10^5$; PS plasma body force: 225 mN/m; SS body force: 450 mN/m.

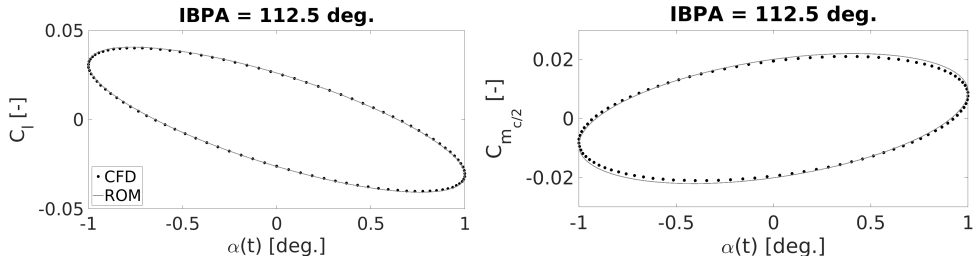

FIGURE 12: Hysteresis curves of lift and moment coefficient for the central blade of the cascade with alternate PS/SS actuation. Interpolation of the ROM parameters at IBPA = 112.5 deg. and CFD simulations performed a a posteriori; off design conditions; Re $\sim 1.9 \times 10^5$; PS plasma body force: 225 mN/m; SS body force: 450 mN/m.

both positive and negative values are found.

Figure 14 shows the equivalent geometry plotted over the nondimensional vorticity field, at four different time steps during the pitching cycle. The ROM reproduces correctly the unsteady near body flow physics, also for the design conditions.

The hysteresis curves of lift and moment coefficients at IBPA of -51.43 deg. and 51.43 deg. are displayed in figure 15. Also in design conditions there is very good agreement between CFD and ROM, for both lift and moment coefficient. The ROM is found to be capable of operating in a predictive manner also in design conditions. In these conditions, the more limited range exhibited by the ROM parameters, allows to get almost always a good prediction of the unsteady airloads for arbitrarily chosen IBPAs. The results of the predictions are not shown here for brevity.

GENERAL REMARKS AND CONCLUSIONS

A physically consistent reduced order model is developed for a compressor cascade equipped with virtual control surfaces. The reduced order model is based on the thin lifting line theory of Küssner and Schwarz. An equivalent three-segment piece-wise mean line is used to reproduce the steady and the unsteady loads on a generic plasma-equipped blade of the cascade. The geometrical and motion parameters of the equivalent geometry are

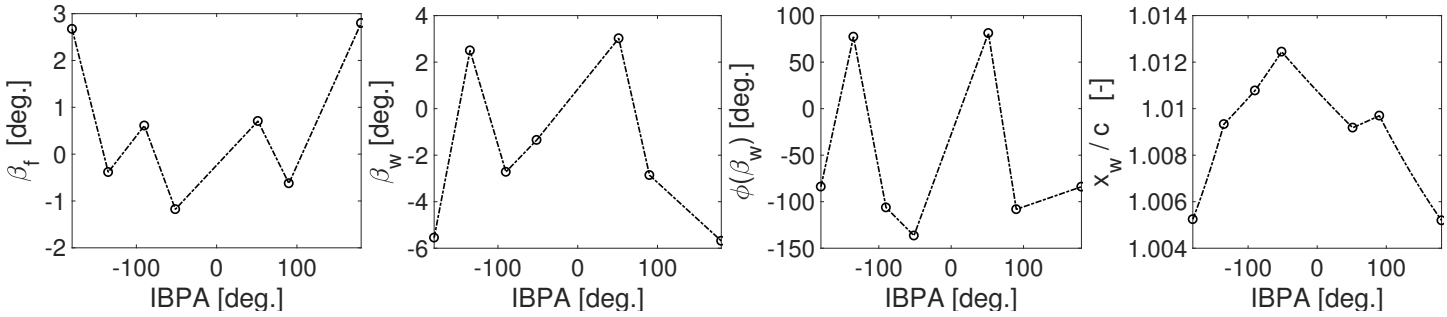

(a) Deflection amplitude of PEF (b) Deflection amplitude of ETT (c) Phase angle of ETT (d) Lenght of ETT

FIGURE 13: Parameters of the ROM equivalent geometry; design conditions; k = 0.0720; Re $\sim 3 \times 10^5$; PS plasma body force: 225 mN/m; SS body force: 450 mN/m.

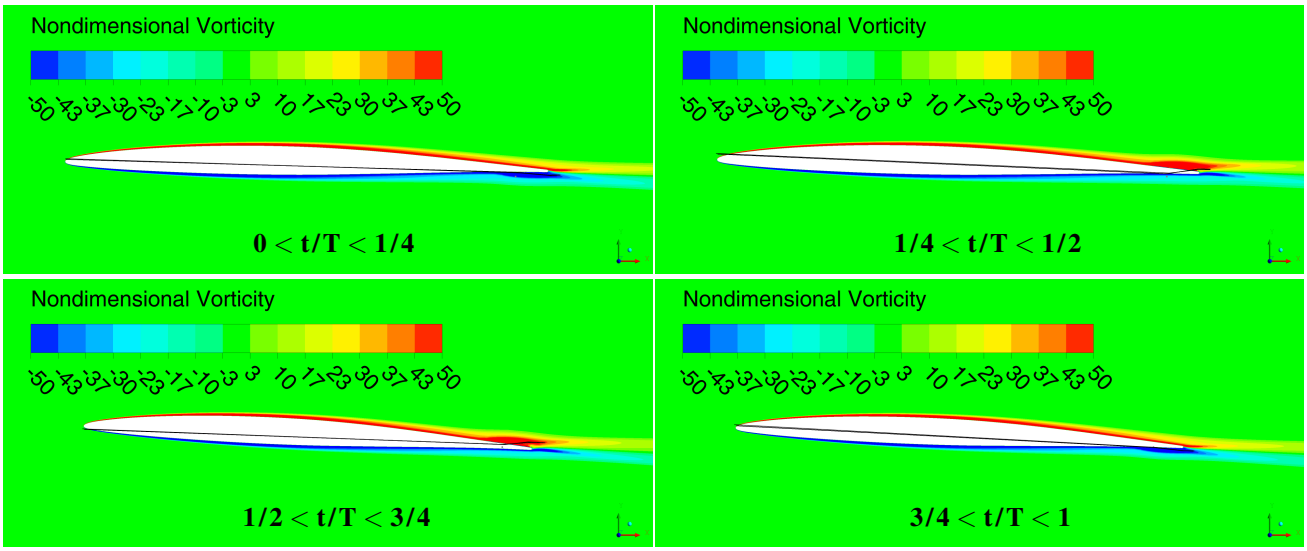

FIGURE 14: Non dimensional vorticity field for the central blade of the cascade with alternate PS/SS actuation, together with the equivalent geometry computed with the ROM; design conditions; k = 0.0720; Re $\sim 3 \times 10^5$; oscillation amplitude: 1 deg.; PS plasma body force: 225 mN/m; SS body force: 450 mN/m.

computed by a least-squares optimization procedure. Namely, the developed algorithm aims to minimize the difference between the airloads issued from CFD computations and the counterparts obtained with the low-order model. It is found that, with as much as two/four degrees of freedom, it is possible to compute and predict accurately the steady/unsteady loads of the plasma equipped cascade. The model takes into account also the effects on loads induced by the neighboring blades. Because the aerodynamic damping can be directly computed as the integral loop of the pitching moment hysteresis curve, the present model can be used also to estimate the aeroelastic stability of the cascade. The reduced order model works for both design and off design conditions, where indeed plasma actuators are expected to operate. Moreover the equivalent geometry reproduces very well the modification in the effective camber line induced by the actuators, particularly at the lower reduced frequency taken under consideration. That is, the reduced order model captures correctly the near body flow physics induced by the conceived actuation system. The capability of predicting accurately the steady and unsteady loads – especially for low reduced frequencies – of the plasma equipped cascade is a powerful tool for sensitivity studies on the configuration of the actuators and on their operation in different flow conditions. The possibility of a straightforward computation of the aerodynamic response enables to enlarge significantly the parameter space for the sensitivity analyses. It is ultimately possible to perform large-scale optimization studies – on the size, location and actuation laws of plasma. Genetic algorithms, tremendously demanding when coupled to CFD simulations, could be rapidly built-up and carried out on the reduced order model developed here. Additionally, the present frequency domain model is suit-

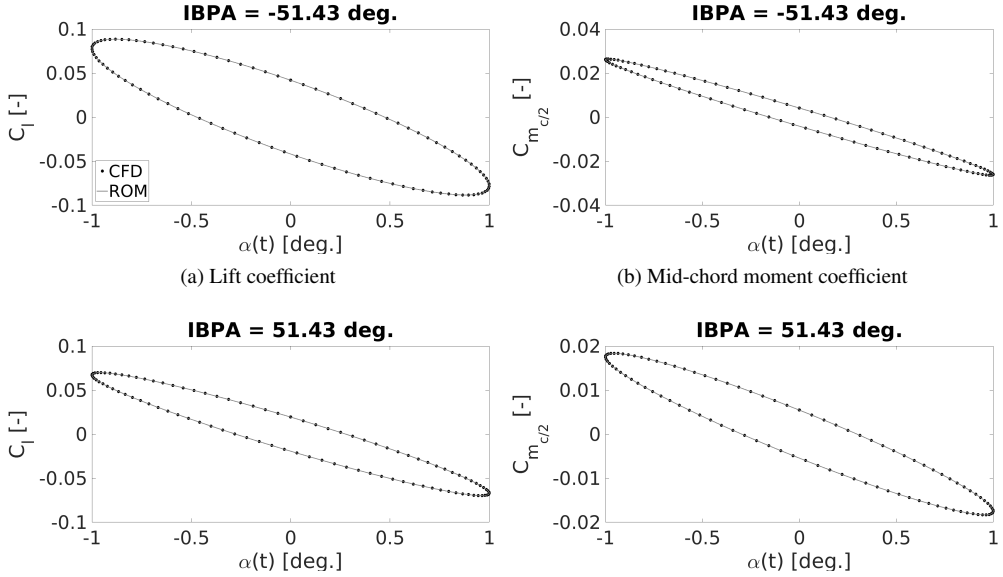

(a) Lift coefficient

(b) Mid-chord moment coefficient

(c) Lift coefficient

(d) Mid-chord moment coefficient

FIGURE 15: Hysteresis curves of lift and moment coefficient for the central blade of the cascade with alternate PS/SS actuation, together with the counterpart of the ROM; design conditions; k = 0.0720; Re $\sim 3 \times 10^5$; PS plasma body force: 225 mN/m; SS body force: 450 mN/m.

able for couplings with low order – e.g. lumped parameters – structural representations. Therefore it allows for carrying out rapidly preliminary aeroelastic assessments, to calculate flutter parameters and to assess the sensitivity of the actuated blade to the structural properties of the cascade. Furthermore, it is possible to perform additional optimization studies for the parameters of the actuation law, by taking into account also the structural response of the cascade. The physical consistency of this reduced order model may have several advantages, compared to black box identification procedures, e.g. rational functions approximations. Indeed it allows to estimate the loads associated to an actuation system, by simply evaluating the impact of the device on the near-body flow field. The availability of information on the near body flow field can be very important for the conceptual and preliminary design of an active control system on a turbomachinery cascade. It is also worth noting that the proposed model is easily extensible to any other control system which operates by modifying the effective sectional shape of a blade or of a generic lifting surface. Flow blowing/suction, piezo-electric or mechanic morphing, adaptable leading edge, Gurney flaps or other flap-like devices are only a few of the actuation systems that could be suitable for this simple, low-order, frequency domain approach to get the aerodynamic response of an actuated lifting surface operating under small perturbation conditions.

ACKNOWLEDGMENTS

The authors gratefully acknowledge the support of the Deutsche Forschungsgemeinschaft (DFG) as part of the collaborative research center CRC 1029 “Substantial efficiency increase in gas turbines through direct use of coupled unsteady combustion and flow dynamics”, Project B01. The support of the Berlin International Graduate School in Model and Simulation based Research (BIMoS) is also warmly recognized.

NOMENCLATURE

a_n	n-th coefficient for the analytical computation of loads
b	blade semi-chord for the analytical model [m]
c	blade chord for the numerical model [m]
c_k	blade chord for the analytical model [m]
C_d	drag coefficient
$C(k)$	Theodorsen function
C_l	lift coefficient
C_m	pitching moment coefficient
C_P	pressure coefficient
f	frequency [Hz]
F	functional to be minimized for the model order reduction
F_a	generic aerodynamic force [N]
g	space dependent upwash velocity within the analytical model
h	airfoil position for the plunge motion [m]
$\Im$	imaginary part of a generic complex parameter
k	reduced frequency, $\omega b/U_\infty$
L	sectional lift coefficient [N/m]
M_0	sectional moment coefficient about the point x_0 [N]
$\mathbf{p}$	array of free parameters for the model order reduction
P_n	upwash n-th coefficient for the analytical model
$\Re$	real part of a generic complex parameter
Re	chord-based freestream Reynolds number
t	time [s]

U_∞ freestream velocity [m/s]
v vertical component of the perturbation velocity [m/s]
x position along the chord within the analytical model [m]
z position coordinate perpendicular to the chord [m]
$\tilde{(\cdot)}$ variables in the Fourier transform domain
α angle of attack [deg.]
β PEF or ETT deflection angle, positive upward [deg.]
φ phase of a generic complex quantity.
ΔC_P difference of C_P between the lower and the upper side
Ξ aerodynamic damping [-]
θ x-transformation coordinate, $x = \cos\theta$
x_w chord extension relative to the physical blade
ω circular frequency [1/s]

Subscript
0 pole of the pitching moment
a quantity related to the aerodynamic forces
k quantity related to the analytical model
KS Küssner-Schwarz
n index for the series terms within the analytical model
N number of terms of the series within the analytical model
f quantity related to the PEF within the analytical model
w quantity related to the ETT within the analytical model

Acronym
CFD Computational Fluid Dynamic(s)
EB Equivalent blade
ETT Equivalent Trim Tab
ELT Equivalent L-Tab
IBPA InterBlade Phase Angle [deg.]
PEF Plasma-Equivalent Flap
PS Pressure Side
ROM Reduced Order Model
SS Suction Side
TE Trailing Edge

REFERENCES

[1] Tiedemann, C., Heinrich, A., and Peitsch, D., 2012. "A New Linear High Speed Compressor Stator Cascade for Active Flow Control Investigations". In 6th AIAA Flow Control Conference, 25—28 June 2012, New Orleans, LA, USA.

[2] Matejka, M., Popelka, L., Safarik, P., and Nozicka, J., 2008. "Influence of Active Methods of Flow Control on Compressor Blade Cascade Flow". In ASME Turbo Expo, 9–13 June 2008, Berlin, Germany, no. GT2008-51109.

[3] Trávníček, Z., Cyrus, V., Šimurda, D., Luxa, M., Lukač, J., and Kordik, J., 2013. "Experimental investigation of the compressor cascade under an active flow control". *EPJ Web of Conferences,* ***45***.

[4] Hammer, S., Phan, D. T., Peter, J., Werder, T., Meyer, R., Liebich, R., and Thamsen, P. U., 2014. "Active flow control by adaptive blade systems in periodic unsteady flow conditions". In Active Flow and Combustion Control, 10–12 September 2014, Berlin, Germany.

[5] Suman, A., Fortini, A., Aldi, N., Merlin, M., and Pinelli, M., 2015. "A Shape Memory Alloy-Based Morphing Axial Fan Blade: Part II — Blade Shape and CFD Analyses". In ASME Turbo Expo 2015: Turbine Technical Conference and Exposition, 15–19 June 2015, Montreal, QC, Canada, no. GT2015-42700.

[6] Suman, A., Fortini, A., Aldi, N., Merlin, M., and Pinelli, M., 2015. "A Shape Memory Alloy-Based Morphing Axial Fan Blade: Part I — Blade Structure Design and Functional Characterization". In ASME Turbo Expo 2015: Turbine Technical Conference and Exposition, 15–19 June 2015, Montreal, QC, Canada, no. GT2015-42695, American Society of Mechanical Engineers.

[7] Monner, H. P., Huxdorf, O., Riemenschneider, J., and Keimer, R., 2015. "Design and manufacturing of morphing fan blades for experimental investigations in a cascaded wind tunnel". In 23rd AIAA/AHS Adaptive Structures Conference, 5–9 January 2015, Kissimmee, FL, USA, no. AIAA 2015-0790, American Institute of Aeronautics and Astronautics.

[8] Phan, D. T. and Springer, P. and Liebich, R., 2017. "Numerical investigation of an elastomer-piezo-adaptive blade for active flow control of a nonsteady flow field using fluid-structure interaction simulations". *Journal of Turbomachinery,* ***139***, pp. 091004–1–091004–10.

[9] Lemire, S., and Vo, H., 2011. "Reduction of fan and compressor wake defect using plasma actuation for tonal noise reduction". *Journal of Turbomachinery,* ***133***(1).

[10] De Giorgi, M. G., Pescini, E., Marra, F., and Ficarella, A., 2014. "Experimental and numerical analysis of a micro plasma actuator for active flow control in turbomachinery". In Proceedings of ASME Turbo Expo 2014: Turbine Technical Conference and Exposition, 16–20 June 2014, Düsseldorf, Germany, no. GT2014-25337, American Society of Mechanical Engineers.

[11] Ashrafi, F., Michaud, M., and Vo, H., 2015. "Delay of rotating stall in compressors using plasma actuators". In ASME Turbo Expo 2015: Turbine Technical Conference and Exposition, 15–19 June 2015, Montréal, QC, Canada, no. GT2015-42559, American Society of Mechanical Engineers.

[12] Sun, X., Jing, X., and Zhao, H., 2001. "Control of blade flutter by smart-casing treatment". *Journal of Propulsion and Power,* ***17***(2), pp. 248–255.

[13] Lu, P., Pan, D., and Yu, Y., 2002. "Acoustic flutter control of three-dimensional transonic rotor flow". *Journal of Propulsion and Power,* ***18***(5), pp. 1003–1011.

[14] Rey, G., Banaszuk, A., and Gysling, D., 2011. "Active control of flutter in turbomachinery using off blade actuators sensors: Experimental results". In ASME 2011 Turbo Expo: Turbine Technical Conference and Exposition, 6–10 June 2011, Vancouver, BC, Canada, American Society of Mechanical Engineers, pp. 1429–1437.

[15] Banaszuk, A., Gysling, D., and Rey, G., 2002. "Active control of flutter in turbomachinery using off blade actuators and

sensors. Part I: Modeling for control". *IFAC Proceedings Volumes,* ***35***(1), pp. 271–276.

[16] Banaszuk, A., Rey, G., and Gysling, D., 2002. "Active control of flutter in turbomachinery using off blade actuators sensors. Part II: Control algorithm". In Proceedings of the 41st IEEE Conference on Decision and Control, 10–13 December 2002, Las Vegas, NV, USA, Vol. 4, pp. 3704–3709.

[17] Angelucci, R. J., Baker, J. R., and Capece, V. R., 2004. "A study on active vibration control for stator vanes in a research compressor". In 40th AIAA/ASME/SAE/ASEE Joint Propulsion Conference and Exhibit, 11–14 July 2004, Fort Lauderdale, FL, USA, no. AIAA 2004-3752, American Institute of Aeronautics and Astronautics.

[18] Motta, V., Malzacher, L., and Peitsch, D., 2017. "Numerical investigation of virtual control surfaces for vibration control on compressor blades". In International Forum on Aeroelasticity and Structural Dynamics, 25–28 June 2017, Como, Italy.

[19] Motta, V., Malzacher, L., Neumann, P., and Peitsch, D., 2017. "Numerical assessment of virtual control surfaces for compressor blades". In AIAA Aviation Forum, 5–9 June 2017, Denver, COL, USA, American Institute of Aeronautics and Astronautics.

[20] Malzacher, L., Geist, S., Peitsch, D., and Hennings, H., 2016. "A low speed compressor test rig for flutter investigations". In Proceedings of ASME Turbo Expo 2016: Turbomachinery Technical Conference and Exposition, 12–16 June 2016, Seoul, South Korea, no. GT2016-57960.

[21] Motta, V., and Quaranta, G., 2015. "Linear Reduced-Order Model for Unsteady Aerodynamics of an L-Shaped Gurney Flap". *Journal of Aircraft,* ***52***, pp. 1887–1904.

[22] Belz, J. and May, M. and and Siemann, J. and Seume, J. R. and Voigt, C. and Böhmer, H. and Grüber, B., 3–7 June 2013. "Excited blade vibration for aeroelastic investigations of a rotating blisk using piezo-electric macro fiber composites". In ASME Turbo Expo 2013: Turbine Technical Conference and Exposition, San Antonio, TX, USA.

[23] Iwrey, B. M., 2016. Gas turbine engine with rotor blade clearance flow control, 06.

[24] Lane, F., 1956. "System mode shapes in the flutter of compressor blade rows". *Journal of the Aeronautical Sciences,* ***23***(1), pp. 54–66.

[25] Carta, F. O., 1982. An Experimental Investigation of Gapwise Periodicity and Unsteady Aerodynamic Response in an Oscillating Cascade. Contractor Report 3523, NASA, United Technologies Research Center.

[26] Sachs, W., 1990. Windkanal für instationäre Gitter (WiG), Messstrecke für instationäre Gitter (MiG). Phase 1: Bau und InbetriebnahmeWindkanal für instationäre Gitter (WiG). Technical report, DLR.

[27] Hennings, H., 1997. "Flutter investigations on a finite linear 2D compressor cascade in a wind tunnel in incompressible flow". PhD thesis, RWTH Aachen.

[28] Whitehead, D. S., 1960. Force and Moment Coefficients for Vibrating Aerofoils in Cascade. Reports and Memoranda 3254, Aeronautical Research Council.

[29] Platzer, M. F., and Carta, F. O., 1987. AGARD Manual on Aeroelasticity in Axial-Flow Turbomachines, Volume 1, Unsteady Aerodynamics. AGARD 298, NASA.

[30] Motta, V., and Quaranta, G., 2016. "A comparative assessment of vibration control capabilities of a L-shaped Gurney flap". *The Aeronautical Journal,* ***120***(1233), pp. 1812–1831.

[31] Keerthi, M. C. and Shubham, S. and Kushari, A., 2017. "Aerodynamic influence of oscillating adjacent airfoils in a linear compressor cascade". *AIAA Journal,* ***55***(12), pp. 4113–4126.

[32] Carta, F. O., 1983. "Unsteady Aerodynamics and Gapwise Periodicity of Oscillating Cascaded Airfoils". *Journal of Engineering for Power,* ***105***(2), July.

[33] Küssner, H., and Schwarz, L., 1941. The oscillating wing with aerodynamically balanced elevator. TM 991, NACA. Translated from Luftfahrtforschung, vol. 17, pp. 337–354, 1940.

[34] Fung, Y., 1955. *Theory of Aeroelasticity*. John Wiley and Sons, Inc., New York.

[35] Verdon, J. M. and Caspar, J. R., 1984. "A linearized unsteady aerodynamic analysis for transonic cascades". *Journal of Engineering for Power,* ***149***(2), July, pp. 403–429.

[36] Leishman, J. G., 2006. *Principle of Helicopter Aerodynamics*. Cambridge University Press, New York, NY, USA.

[37] Theodorsen, T., 1935. General Theory of Aerodynamic Instability and the Mechanism of Flutter. TR 496, NACA.

[38] Motta, V., Guardone, A., and Quaranta, G., 2015. "Influence of airfoil thickness on unsteady aerodynamic loads on pitching airfoils". *Journal of Fluid Mechanics,* ***774***, pp. 460–487.

[39] Liu, T., and Montefort, J., 2007. "Thin-Airfoil Theoretical Interpretation for Gurney Flap Lift Enhancement". *Journal of Aircraft,* ***44***(2), Mar.

[40] Katz, J. and Plotkin, A., 2010. *Low-Speed Aerodynamics*. Cambridge University Press, New York, NY, USA.